Z. Phys. C – Particles and Fields 47, 1–10 (1990)

Zeitschrift für Physik C Particles and Fields

Measurement of inclusive γ, π^0, and η production in e^+e^- annihilation at $\sqrt{s}=35$ GeV

CELLO Collaboration

H.J. Behrend, L. Criegee, J.B. Dainton[1], J.H. Field[2], G. Franke, H. Jung[3], J. Meyer, V. Schröder, G.G. Winter
Deutsches Elektronen-Synchrotron, DESY, Hamburg, Federal Republic of Germany

P.J. Bussey, C. Buttar[4], A.J. Campbell, D. Hendry, J.M. Scarr, I.O. Skillicorn, K.M. Smith
University of Glasgow, Glasgow, UK

J. Ahme, V. Blobel, W. Brehm, M. Feindt, H. Fenner, J. Harjes, J.H. Peters, O. Podobrin, H. Spitzer
II. Institut für Experimentalphysik, Universität, Hamburg, Federal Republic of Germany

W.D. Apel, J. Engler, G. Flügge[3], D.C. Fries, J. Fuster[5], P. Gabriel, K. Gamerdinger[6], P. Grosse-Wiesmann[7], M. Hahn, U. Hädinger, J. Hansmeyer, H. Küster[8], H. Müller, K.H. Ranitzsch, H. Schneider, R. Seufert
Kernforschungszentrum Karlsruhe und Universität, Karlsruhe, Federal Republic of Germany

W. de Boer, G. Buschhorn, G. Grindhammer[7], B. Gunderson, C. Kiesling[9], R. Kotthaus, H. Kroha, D. Lüers, H. Oberlack, P. Schacht, S. Scholz, G. Shooshtari, W. Wiedenmann
Max-Planck-Institut für Physik und Astrophysik, München, Federal Republic of Germany

M. Davier, J.F. Grivaz, J. Haissinski, P. Janot, V. Journé, D.W. Kim, F. Le Diberder, J.J. Veillet
Laboratoire de l'Accélérateur Linéaire, Orsay, France

K. Blohm, R. George, M. Goldberg, O. Hamon, F. Kapusta, L. Poggioli, M. Rivoal
Laboratoire de la Physique Nucléaire et Hautes Energies, Université de Paris, Paris, France

G. d'Agostini, F. Ferrarotto, M. Iacovacci, B. Stella
University of Rome and INFN, Rome, Italy

G. Cozzika, Y. Ducros
Centre d'Études Nucléaires, Saclay, France

G. Alexander, A. Beck, G. Bella, J. Grunhaus, A. Klatchko, A. Levy, C. Milstène
Tel Aviv University, Tel Aviv, Israel

Received 27 April 1989; in revised form 12 February 1990

Abstract. We have measured the inclusive production of γ, π^0 and η in e^+e^- annihilation at the center of mass energy of 35 GeV. The differential cross sections, extended to the kinematical limit and measured with high accuracy, are found to be in good agreement with previously reported results. Using the measured spectra we determine the average multiplicity for each of these particle species.

[1] Permanent address: University of Liverpool, UK
[2] Now at Université de Genève, Switzerland
[3] Now at RWTH, Aachen, FRG
[4] Now at Oxford Univ., United Kingdom
[5] Now at Instituto de Física Corpuscular, Universidad de Valencia, Spain
[6] Now at MPI München
[7] Now at SLAC, Stanford, USA
[8] Now at DESY
[9] Heisenberg-Stipendiat der Deutschen Forschungsgemeinschaft

1 Introduction

Investigation of the production of different particle species in e^+e^- collisions has received much attention in

the past few years. Within the framework of the quark-parton model the final state hadrons originate from the primary partons (quarks and gluons) which are produced in the e^+e^- annihilation. However, the underlying mechanism responsible for the fragmentation of the initial partons into hadrons is largely unknown and cannot be calculated perturbatively within QCD, the gauge theory of the strong interaction between quarks and gluons. Since QCD-based predictions are valid only at the parton level, models are needed to describe the transition from the parton state to the hadronic final state. The functional form of the parton evolution, generally referred to as the fragmentation function, incorporates several input parameters which are subject to tuning and vary from model to model. Therefore it is important to have experimental information on the particle composition of the hadronic final states in e^+e^- annihilation. To this end, inclusive distributions and relative abundances of particles are used to study the process of quark and gluon fragmentation into jets of hadrons.

In this paper we present measurements of the scale invariant differential cross sections for γ, π^0 and η in an experiment at $\sqrt{s}=35$ GeV using the CELLO detector at PETRA. Previous results from this experiment on the inclusive γ and π^0 production at lower center of mass energies, based on a substantially lower statistics, have been published elsewhere [1]. After a brief description of the detector and the event selection criteria in Sect. 2, we discuss the photon selection criteria and present the results on inclusive γ spectra in Sect. 3. In Sect. 4 we present results on inclusive π^0 production using two methods of π^0 reconstruction applicable to low and high momenta, respectively. The identification of π^0's at large momenta is facilitated by the fine granularity of the CELLO lead liquid argon calorimater. Finally in Sect. 5, we present results on the inclusive η cross section.

2 Detector and event selection

The CELLO detector has been described elsewhere [2]. We mention here only those parts of the experimental setup most relevant for this analysis.

Charged particles were measured in a tracking system consisting of interleaved cylindrical drift and proportional chambers in a 1.3 T axial magnetic field yielding a momentum resolution of $\sigma(p)/p=2\%\cdot p\cdot\sin\theta$ (p in GeV/c) over 92% of the solid angle. A coarse track recognition between consecutive bunch crossings provides a charged particle trigger.

Photons are detected by reconstruction of their electromagnetic showers in the barrel part of a fine grain lead liquid argon electromagnetic calorimeter which subtends a solid angle of 86% of 4π. The polar angular range $|\cos\theta|\geqq 0.86$ was excluded from this analysis. The barrel calorimeter consists of 16 modules each of which is 21 radiation lengths (X_0) deep and samples the energy deposited by particles in the liquid argon 17 times in depth. The energy is collected on lead strips at three different orientations. For each particle this information is combined into seven energy clusters in depth. In multihadronic final states we obtain an energy resolution of $\sigma(E)/E=12\%/\sqrt{E}$ (E in GeV) and an angular resolution of 4 mrad for photons originating from the interaction point. The energy resolution, however, may deteriorate inside the jets by as much as a factor of two due to the substantial overlap between clusters from different photons as well as between photons and charged particles. Charged and neutral particles are distinguished using the information from the central detector to find links between the charged particle tracks and energy clusters in the calorimeter.

The barrel calorimeter was calibrated using QED events leading to a single e^- or e^+ in the detector. For each module the energy calibration was obtained by comparing the total deposited charge in the shower linked to the charged particle and the momentum as measured in the tracking chambers. One advantage of this method over the use of Bhabha events is that it allows direct energy calibration down to low energies inaccessible with Bhabha scattering. The two methods, however, are found to give consistent results at high energies.

A combination of charged particle and low threshold calorimetric triggers provides an efficient way to detect multihadronic events in CELLO [2]. Data reduction is done online by a filter program which verifies the trigger conditions and removes obvious background. In the off-line analysis, events are accepted as multihadronic if the following requirements are satisfied:

1. at least 5 charged particles each with a transverse momentum $P_t\geqq 150$ MeV/c with respect to the beam axis, reconstructed within the polar angular range $|\cos\theta|\leqq 0.865$ and originating inside a radius of 5 mm around the interaction vertex,
2. the total net charge of all particles in the event less than 7,
3. either: (a) the neutral visible energy measured in the barrel calorimeter of more than 1.0 GeV and the total visible energy of all (charged and neutral) particles in the event greater than $0.33\cdot\sqrt{s}$, or (b) the total visible energy of all particles greater than $0.22\cdot\sqrt{s}$ and at least one charged particle in both the forward and the backward hemispheres with respect to the electron beam.

These cuts efficiently remove contaminations due to $\gamma\gamma$ reactions, $\tau^+\tau^-$ production, cosmic rays and beam gas events. The final data sample consists of 23673 multihadronic events. The residual background is estimated by a visual scan to be less than 3%. The event sample used corresponds to an integrated luminosity of $87\,\mathrm{pb}^{-1}$ as measured using Bhabha scattering in the barrel calorimeter.

The overall detection efficiency and radiative corrections were determined by a detailed simulation of multihadronic events using the LUND model (version 5.2) [3] including second order QCD and initial state bremsstrahlung. The model employed string fragmentation with an optimized set of input parameters (see Table 1) so that the simulated final states closely reproduced the real data. The generated Monte Carlo (MC) events were

Table 1. Parameter values used for event generation with the LUND 5.2 MC program

Matrix element ($O(\alpha_s^2)$ QCD):		
QCD scale parameter	Λ_{QCD}	$=0.5$ GeV
minimal scaled invariant mass of two partons	y	>0.01
transverse fragmentation:		
width of Gaussian transverse momentum distribution	σ_q	$=0.25$ GeV
longitudinal fragmentation:		
LUND fragmentation function for light quarks (u, d, s) $\left(f(z)\sim\frac{1}{z}(1-z)^A\exp\left(-\frac{Bm_T^2}{z}\right)\right)$	A	$=1.0$
	B	$=0.6$ GeV^{-2}
Peterson fragmentation function for heavy quarks (c, b) $\left(f(z)\sim\frac{1}{z}\left[1-\frac{1}{z}-\frac{\varepsilon_{c,b}}{1-z}\right]^{-2}\right)$	ε_c	$=0.025$
	ε_b	$=0.0035$
vector meson fraction for light quarks		0.40
vector meson fraction for heavy quarks		0.75

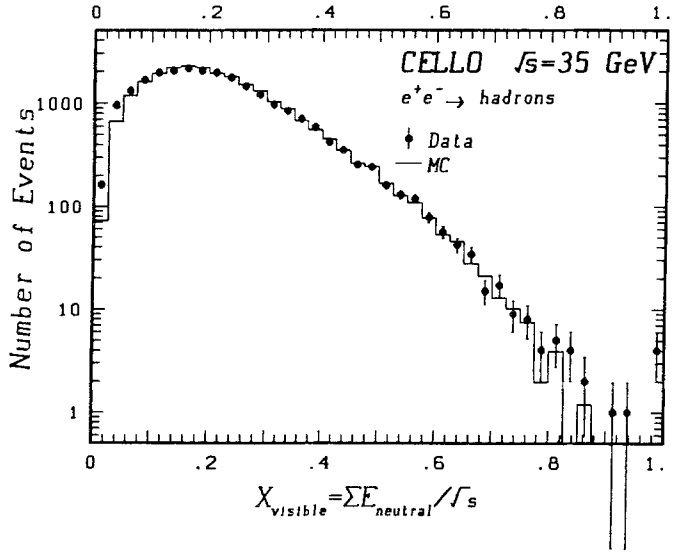

Fig. 1. Distributions of neutral visible energy of multihadronic events in data and MC. The spectra are normalized to the same number of events.

processed through a chain of detector simulations which incorporated all known features of the CELLO detector. Electromagnetic and hadronic interactions of final state particles in the detector components were simulated using the EGS [4] and HETC [5] codes, respectively. Furthermore, the varying experimental and detector conditions during data taking were taken into account by simulating events accordingly. The MC events were processed using the same selection and reconstruction criteria as for the real data. From MC studies we find the detection efficiency of multihadronic events to be 72%, with the acceptance cut being the most important cause of loss of events. In Fig. 1 we show a comparison of visible neutral particle energy fractions in accepted multihadronic events for data and MC. We observe a very good agreement indicating that the overall features of the data and the experimental apparatus are properly simulated in the MC. The spectra are normalized to the same number of events.

3 Inclusive photon production

Showers of at least 200 MeV energy in the calorimeter are considered as photons if they have no link to a charged particle track and satisfy the following additional requirements:

1. the fraction of deposited charge in the 2nd and 3rd layers of the liquid argon calorimeter, extending from 3 to $8X_0$, is in excess of 15% of the total charge of the shower, and the fraction in the last layer ($>16X_0$) is less than 5%,
2. at least three consecutive layers of the calorimeter have to contain clusters of energy,
3. complete containment in one module: Neutral showers extending to neighbouring modules are rejected, and in addition the polar angle of the shower must lie within the fiducial volume of a calorimeter module defined by $0.04<|\cos\theta|<0.84$,
4. "photons" resulting from three or more overlapping showers are rejected and from the remainder of overlapping showers we accepted only those that result in a *double cluster* in the 2nd and 3rd layers of the calorimeter. These layers have fine lateral segmentation and provide an efficient way for separating nearby showers. The average strip width in these layers of the calorimeter modules is about 2 cm.

The identification of electromagnetic showers over a wide range of energies is achieved by applying the first two cuts described above with the second cut being the most severe requirement for low-energy photon identification. Hadrons interacting inside the calorimeter generally produce clusters of energy in the rear layers which are efficiently rejected by the first of the shower shape cuts.

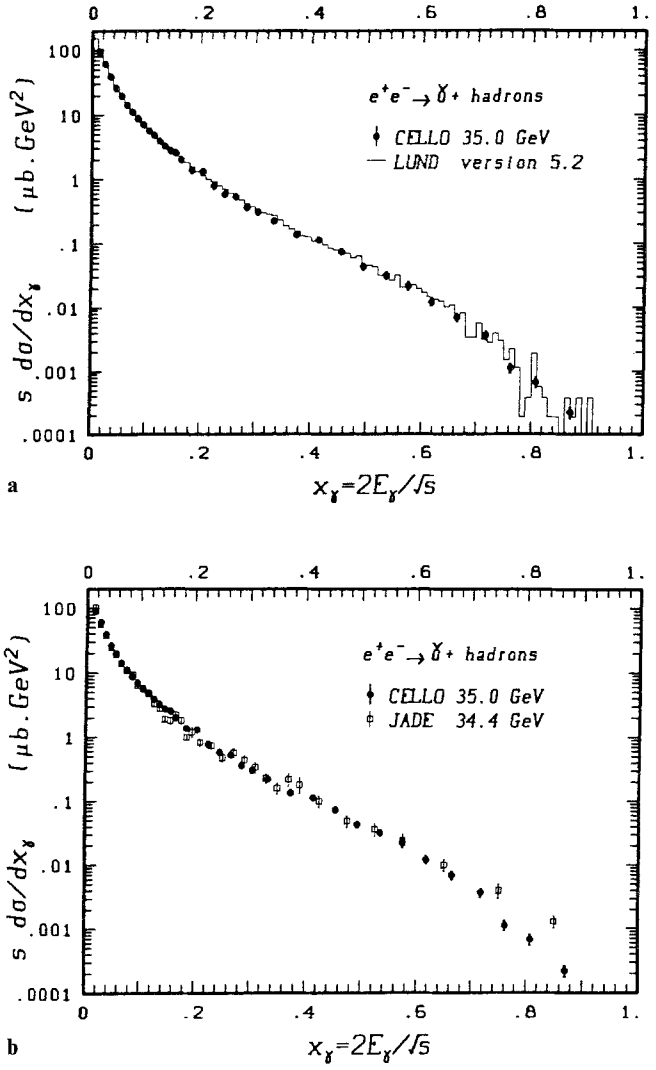

Fig. 2a, b. The scale invariant differential cross section for photon production: **a** comparison with MC predictions, **b** comparison with measurements of the JADE experiment

Based on the MC studies we obtain an average photon reconstruction efficiency of 22% for photon energies above 0.5 GeV. This low efficiency is mainly caused by the strong overlap of particles due to the jet structure of multihadronic events. The background due to misidentified neutrons, K_L, or unlinked charged particles is estimated to be less than 1%. The scale invariant inclusive differential cross section for photon production at $\sqrt{s}=35$ GeV, $s\frac{d\sigma}{dx_\gamma}$ where $x_\gamma=E_\gamma/E_{\text{beam}}$, is shown in Fig. 2a and listed in Table 2. These cross sections have been corrected for acceptance and initial state radiation using the detailed MC simulation described in the previous section. Only statistical errors are given. The various contributions to the systematic errors are energy calibration (3%), MC simulation (3%), normalization (2%), and photon selection (3%). The latter contribution is obtained by varying shower shape parameters over a wide range and is a mean value over the full energy spectrum. Near the extreme ends of the spectrum this

Table 2. The scale invariant differential cross sections for inclusive production of γ's in e^+e^- annihilation at $\sqrt{s}=35$ GeV. Errors are statistical only. See text for systematic errors

x_γ	$s\frac{d\sigma}{dx_\gamma}$ ($\mu b\cdot\text{GeV}^2$)	x_γ	$s\frac{d\sigma}{dx_\gamma}$ ($\mu b\cdot\text{GeV}^2$)
0.015	89.61 ± 1.00	0.225	$0.77\ \pm0.06$
0.025	60.90 ± 0.63	0.245	$0.58\ \pm0.05$
0.035	39.11 ± 0.48	0.265	$0.53\ \pm0.05$
0.045	26.11 ± 0.39	0.285	$0.36\ \pm0.04$
0.055	19.60 ± 0.35	0.305	0.309 ± 0.034
0.065	14.10 ± 0.30	0.333	0.224 ± 0.018
0.075	11.00 ± 0.28	0.374	0.135 ± 0.012
0.085	8.68 ± 0.25	0.414	0.112 ± 0.011
0.095	7.02 ± 0.24	0.454	0.073 ± 0.008
0.105	5.63 ± 0.22	0.493	0.043 ± 0.005
0.115	4.79 ± 0.20	0.535	0.032 ± 0.004
0.125	3.89 ± 0.18	0.575	0.022 ± 0.003
0.135	3.24 ± 0.17	0.618	0.012 ± 0.002
0.145	2.75 ± 0.16	0.664	0.007 ± 0.001
0.155	2.54 ± 0.16	0.718	0.0037 ± 0.0006
0.165	1.99 ± 0.10	0.762	0.0011 ± 0.0002
0.185	1.37 ± 0.09	0.808	0.0007 ± 0.0001
0.205	1.31 ± 0.08	0.870	0.0002 ± 0.0001

error is higher compared to the central region due to reconstruction difficulties for low energy photons (low x) and overlapping photons from high energy π^0's (high x), respectively.

When compared with the cross section given by the LUND model (histogram in Fig. 2a), we observe very good agreement within the measured energy range thus giving confidence in using the MC spectrum to extrapolate to the experimentally inaccessible energy region $x_\gamma<0.01$. In Fig. 2b our experimental results are also compared with measurements of the JADE experiment [6] at a similar center of mass energy. The two measurements agree with each other for $x_\gamma<0.7$, but they disagree at high x_γ.

The observed inclusive photon cross section can be used to arrive at the average photon multiplicity $\langle N_\gamma\rangle$ and also the average energy fraction carried by photons $\langle f_\gamma\rangle$ in multihadronic events:

$$\langle N_\gamma\rangle=\frac{1}{\sigma_{\text{tot}}}\int_0^1\left(\frac{d\sigma}{dx_\gamma}\right)dx_\gamma$$

$$\langle f_\gamma\rangle=\frac{1}{2\sigma_{\text{tot}}}\int_0^1 x_\gamma\left(\frac{d\sigma}{dx_\gamma}\right)dx_\gamma,$$

where σ_{tot} is the total hadronic cross section measured in the same experiment [7]. Based on the MC calculations the contribution from the unobserved cross section ($x_\gamma<0.01$) is 45.8% of the measured ($x_\gamma>0.01$) cross section. Thus evaluating the integrals for the full energy domain we obtain $13.6\pm0.3\pm0.8$ for the average photon multiplicity and $0.267\pm0.017\pm0.017$ for the average energy fraction carried by photons in multihadronic events, in good agreement with previous measurements [2, 6, 8]. The systematic errors also include the uncertainties due to the MC extrapolation to the full x range.

4 Inclusive π^0 production

We have used two different but complementary methods for neutral pion reconstruction depending on the energies involved: In the first method, applicable to low energies ($E_{\pi^0} < 9$ GeV), π^0's are identified by forming the invariant mass of the reconstructed photon pairs, whereas in the second method the shape of high energy showers ($E_{\pi^0} > 5$ GeV) in the calorimeter is used to discriminate π^0's against single photons. The energy region of overlap in both methods, i.e. $5.0 \leqq E_{\pi^0} < 9.0$ GeV, serves as a consistency check on the reconstruction techniques.

4.1 Low energy method

In each event reconstructed photons (as described in Sect. 3) with a minimum energy of 350 MeV were accepted and an invariant mass for each photon pair was calculated. To reduce the combinatorial background the combination of photons originating from different overlapping showers were rejected. The invariant mass distribution of the remaining $\gamma\gamma$ combinations is displayed in Fig. 3. A clear π^0 signal with a peak value at 135 MeV/c^2 is observed. The corresponding MC distribution (solid histogram in Fig. 3), normalized to the number of accepted multihadronic events in the data, is found to be in good agreement with the data. Normalizing to the number of entries in the interval $270 \leqq m_{\gamma\gamma} \leqq 470$ MeV/c^2 leads to agreement with the former within 5%.

The background under the π^0 peak has been determined in two ways: First, reconstructed photon pairs not originating from the same parent π^0 are used to estimate the combinatorial background (dashed histogram in Fig. 3). As an alternative way of estimating the background, the $\gamma\gamma$ mass spectrum of the data in the interval $20 \leqq m_{\gamma\gamma} \leqq 400$ MeV/c^2 was fitted with a Gaussian distribution for the π^0 signal on top of a polynomial

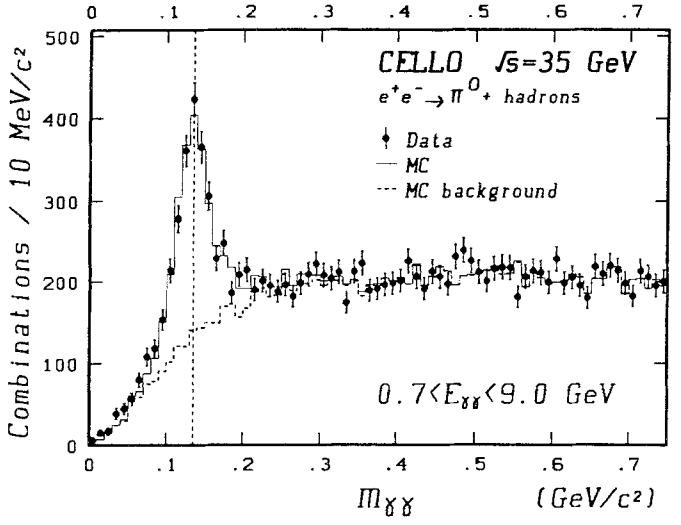

Fig. 3. The invariant mass distribution of $\gamma\gamma$ combinations for data (full circles), MC (solid histogram) and background (dashed histogram)

curve for the background. In the fit the width and the central value of the Gaussian were treated as free parameters. Results of the fit for signal and background are depicted in Fig. 4a–c for different π^0 energy intervals. A mean value for the π^0 mass of 136.1 ± 1.1 MeV/c^2 and a width of $\sigma_m = 20.7 \pm 1.4$ MeV/c^2 are obtained, consistent with our energy resolution.

Both methods of background determination agree with each other. The latter method, however, is used to determine the background under the π^0 peak in order to avoid possible systematic errors introduced by the MC simulation and background estimation. The background-subtracted distributions of $m_{\gamma\gamma}$ are shown in Fig. 4d–f. The total number of π^0's (signal region $60 \leqq m_{\gamma\gamma} \leqq 210$ MeV/c^2) in the energy range $0.7 \leqq E_{\pi^0} < 9.0$ GeV is $n_{\pi^0} = 1267 \pm 91$ where the error includes the uncertainty in the background subtraction.

The energy dependence of the observed π^0 efficiency (defined as the ratio of reconstructed to generated π^0's) exhibits a maximum corresponding to about 4% around 1.5 GeV, smoothly falling at higher energies where, due to the small opening angles of the decay products, the efficiency for reconstructing both photons is reduced. The average π^0 efficiency is 2.8%.

4.2 High energy method

Photons resulting from the decay of a high energy π^0 produce showers in the calorimeter which substantially overlap in their longitudinal as well as lateral structures. The resultant energy clusters are frequently merged to an extent that they can no longer be separated into two isolated showers and thus superficially appear as a single shower. Making use of the fine granularity of the CELLO calorimeter we employed an algorithm which efficiently identified such π^0's up to the highest energies. This was done by analyzing the energy clusters in the 2nd and 3rd layers of the calorimeter having the finest spatial resolution. For each of these layers, the raw pulse-height distributions in orthogonal projections were searched for a possible double peak structure in the shower. In addition, the lateral spread of the shower was also used as a criterion to distinguish overlapping electromagnetic showers from single ones where the algorithm failed to identify the double peak structure. In order to reduce possible contributions due to electronic noise a minimum energy corresponding to about 10 MeV was required for the individual read-out strips making up the cluster in each projection.

π^0's were identified as follows:

- Showers with at least one unambiguous double peak (with a minimum separation of 1 strip) in any of the projections are accepted as π^0. Various requirements such as a minimum pulse height of the dip between the shower peaks or a minimum number of consecutive strips in each projection were also imposed in order to efficiently eliminate the effects produced by malfunctioning strips and shower fluctuations. MC studies of multihadronic final states show that about 45% of incident

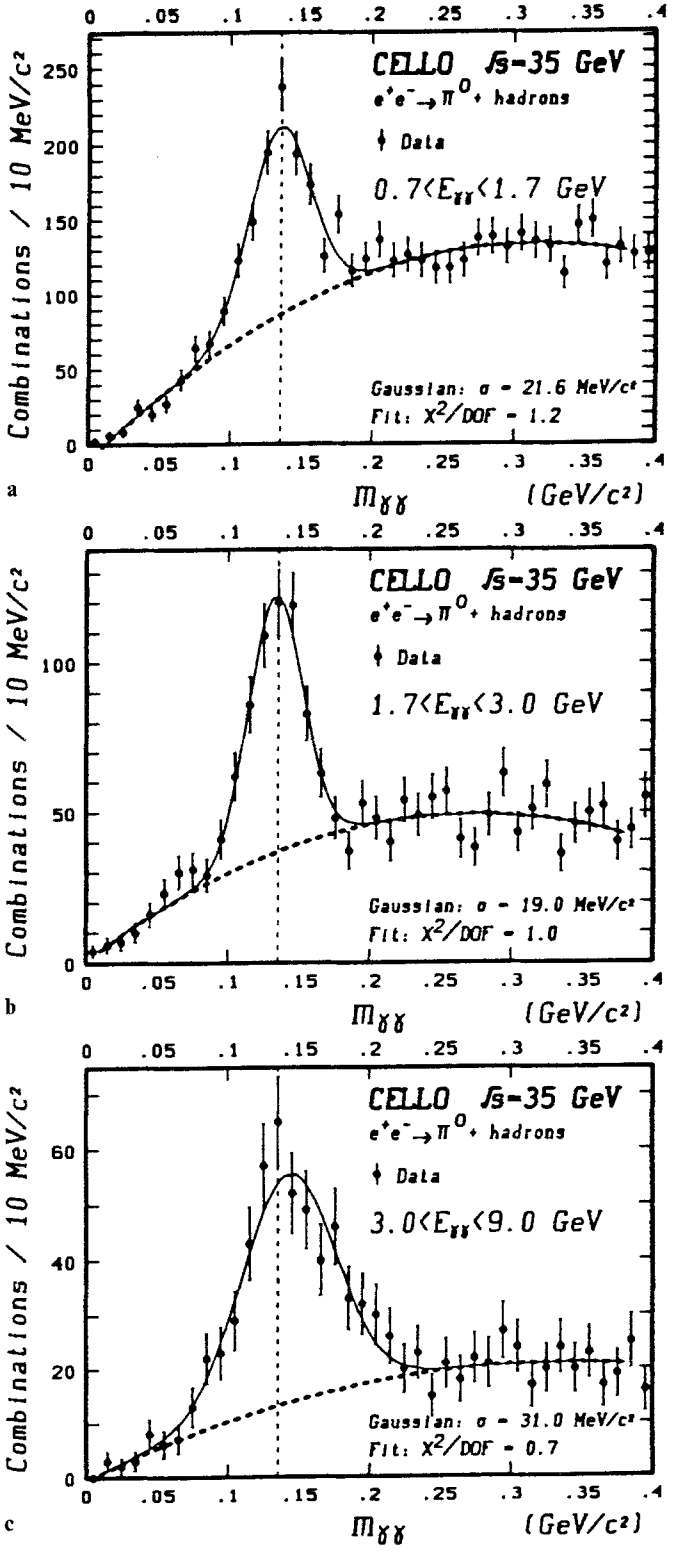

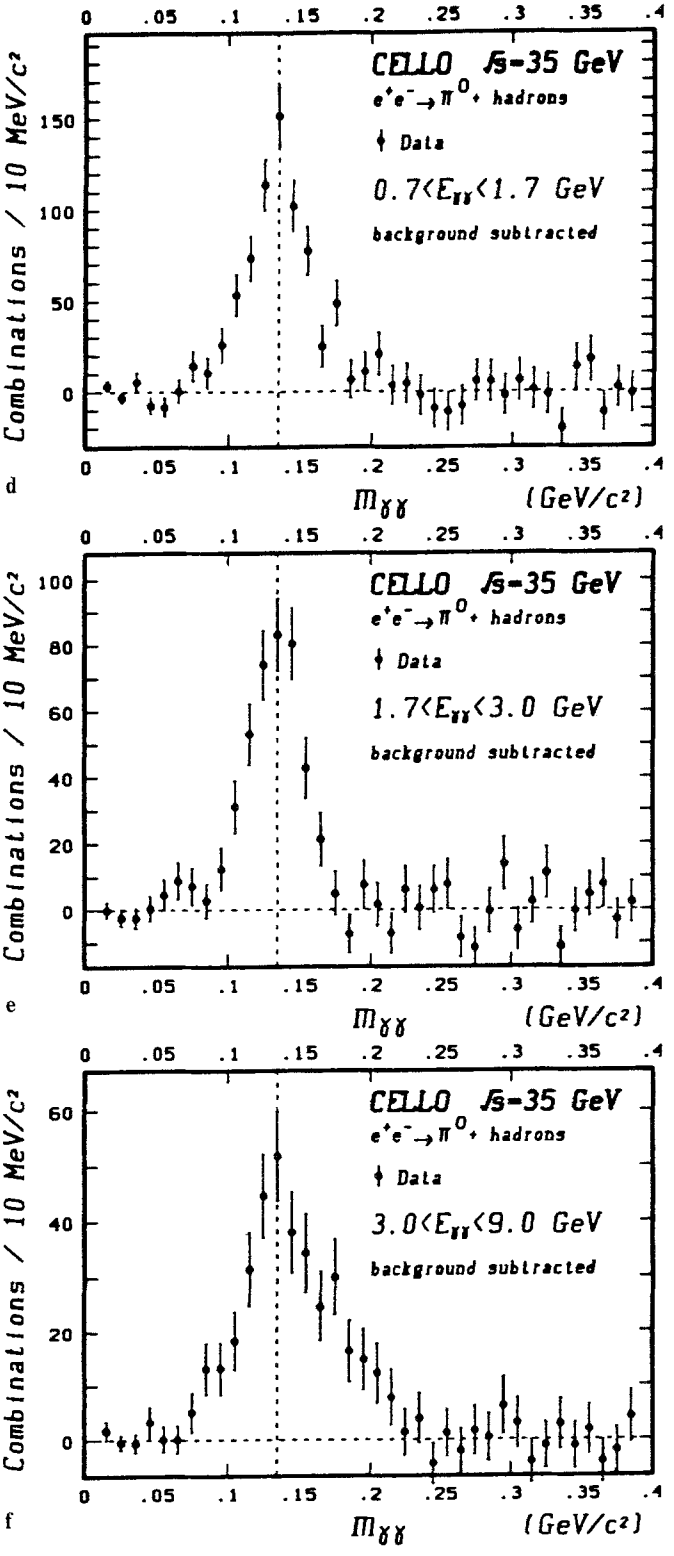

Fig. 4a–f. The invariant mass distribution of $\gamma\gamma$ combinations for different ranges of π^0 energy: **a–c** Data (full circles), Gaussian (solid curve) and polynomial fit (dashed curve) to signal and background, respectively, **d–f** Data after background subtraction

π^0's with $E_{\pi^0} \geqq 5$ GeV can be identified in this way with a background of less than 5% due to single photon showers.

- The highly correlated lateral widths of the energy clusters in layers 2 and 3, $\sigma_{2,3}$, are summed together in order to reduce possible shower fluctuations and to further enhance the difference between broad and narrow showers. Showers are accepted as π^0 if $\sigma_2 + \sigma_3 \geqq 3.5$ cm, provided at least a total of 7 strips contributed to the energy clusters each with pulse-height above 20% of the

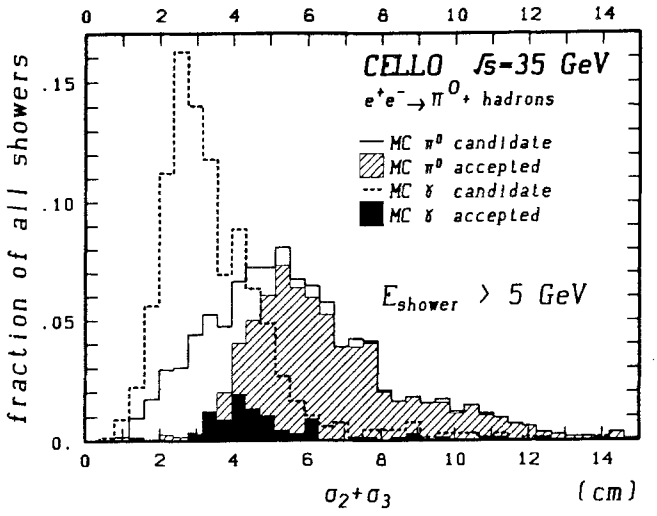

Fig. 5. Distributions of lateral widths of candidate and accepted high energy MC showers due to single γ's and π^0's in the CELLO calorimeter

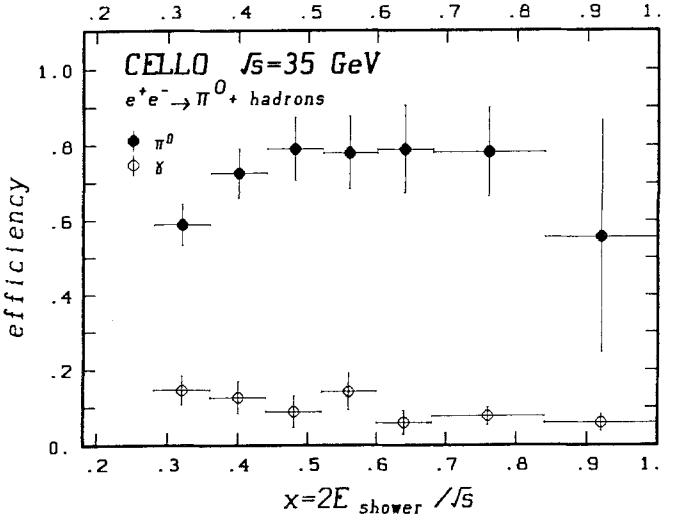

Fig. 7. Efficiency as a function of fractional energy for high energy showers.

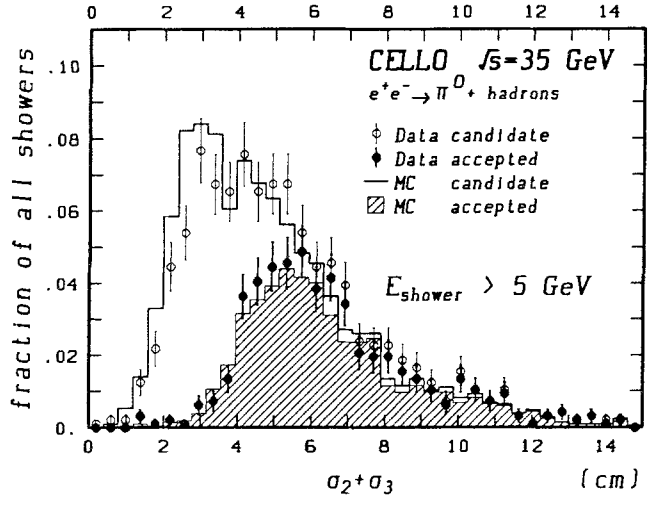

Fig. 6. Distributions of lateral widths of high energy showers in data and MC

maximum pulse-height in both layers. The σ_i's are corrected for polar angle dependence using a polynomial parameterization in the range $|\cos\theta| \leqq 0.84$. This small correction is necessary because obliquely incident photons encounter more detector material thus leading to showers which are broader in the front layers.

There is a large overlap between the two ways of high-energy π^0 identification described above. The combined selection criteria lead to a γ/π^0 suppression factor in excess of 8, well above the previously quoted experimental values [9]. This enables us to discriminate π^0 showers against those of single photons up to the kinematical limit.

MC distributions of $\sigma_2+\sigma_3$ for π^0's and also for single photons with reconstructed shower energies above 5 GeV are compared in Fig. 5, whereas in Fig. 6 we show a comparison of data and MC. All distributions have been normalized to the total number of candidate showers of each type. The observed agreement both in shape and total yield between the data and MC supports the correctness of shower as well as detector simulations at high energies which is essential for such an analysis. Separating the π^0 component of the accepted MC showers indicates that the background is small (less the 10%). In Fig. 7 we show the energy dependence of the efficiency (the ratio of accepted to candidate showers) for π^0's and γ's, respectively.

The remaining background in the sample of accepted π^0's is composed of three categories of showers with different origins. Single photons due to initial state radiation and from asymmetric decays of π^0's and η's, where only one of the decay photons is reconstructed, make up 65% of the background. In the second category we include two photon decays of high energy η mesons, which produce broad showers in the detector indistinguishable from those of π^0's. Such showers amount to 30% of the total background. The remainder of the background is attributed to showers from other sources such as misidentified particles.

4.3 Differential cross section for inclusive π^0 production

Figure 8a shows the scale-invariant differential cross section for π^0 production after correction for initial state radiation as derived from the low and high energy methods described in Sects. 4.1 and 4.2, respectively. Only statistical errors are shown. The estimated systematic errors rise with x from 12% to 15% for the low energy method, and from 5% to 15% for the high energy method.

In the energy range of overlap the two methods of π^0 reconstruction agree with each other and both are found to be well described by the expectation from the LUND model which is shown as a histogram in Fig. 8a. Tables 3 and 4 summarize the cross section measurements which agree well with our previous analysis [1].

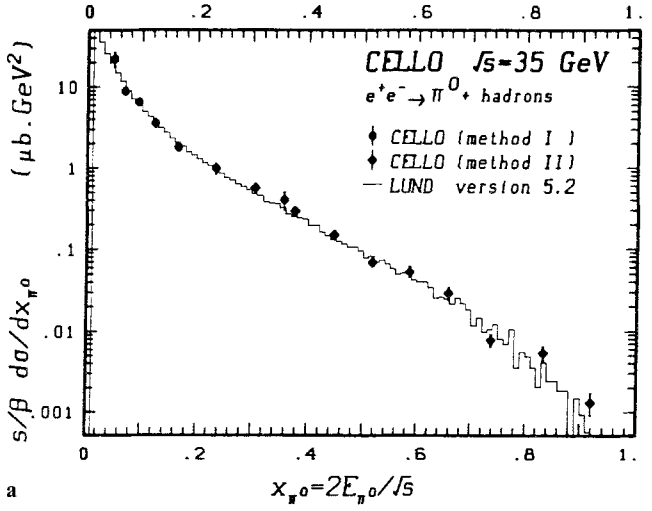

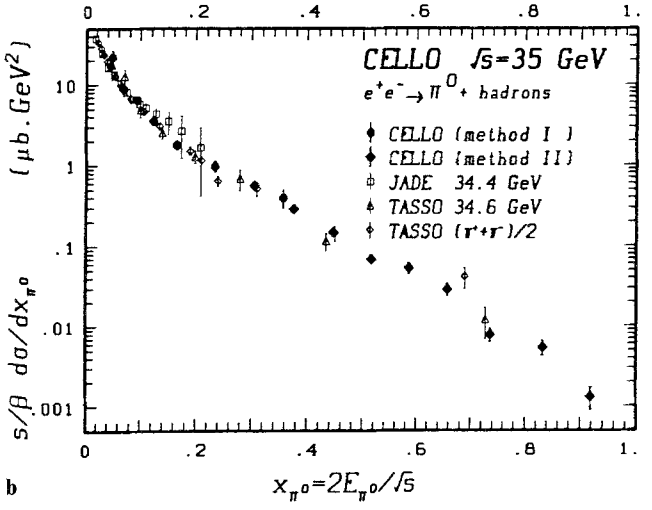

Fig. 8a. The scale invariant differential cross section for inclusive low and high energy π^0 production, **b** comparison of π^0 measurements from experiments at PETRA

Table 3. The scale invariant differential cross sections for inclusive π^0 production at low energies ($0.7 \leqq E_{\pi^0} < 9.0$ GeV) in e^+e^- annihilation at $\sqrt{s} = 35$ GeV. Errors are statistical only. See text for systematic errors

x_{π^0}	$\frac{s}{\beta}\frac{d\sigma}{dx_{\pi^0}}$ ($\mu b \cdot \mathrm{GeV}^2$)
0.049	22.098 ± 4.508
0.069	8.845 ± 0.905
0.094	6.484 ± 0.710
0.124	3.564 ± 0.432
0.166	1.797 ± 0.217
0.235	0.979 ± 0.143
0.358	0.396 ± 0.098

A comparison of these results with other experiments [6, 9] is also shown in Fig. 8b. The results presented here extend previous measurements of π^0 production to higher momenta.

Using the definition given in Sect. 3, the average π^0 multiplicity per event in the range $0.04 \leqq x_{\pi^0} < 1.0$ is found to be $\langle N_{\pi^0} \rangle = 3.42 \pm 0.32 \pm 0.41$. The corresponding expectation from the LUND model yields 3.49 for the production of π^0's in the same energ range. Assuming the model predictions to be also a good description of very low energy neutral pion production, we obtain $\langle N_{\pi^0} \rangle = 6.43 \pm 0.60 \pm 0.86$ for the full energy range $M_{\pi^0} < E_{\pi^0} < E_{\mathrm{beam}}$. The systematic error includes the uncertainty due to the MC extrapolation to the full x range. In the extrapolation procedure the data were corrected for events below $x_{\pi^0} < 0.04$ using the LUND model. The LUND prediction yields 6.57 for the average π^0 multiplicity in the same range.

Table 4. The scale invariant differential cross sections for inclusive π^0 production at high energies ($E_{\pi^0} > 5.0$ GeV) in e^+e^- annihilation at $\sqrt{s} = 35$ GeV. Errors are statistical only. See text for systematic errors

x_{π^0}	$\frac{s}{\beta}\frac{d\sigma}{dx_{\pi^0}}$ ($\mu b \cdot \mathrm{GeV}^2$)
0.306	0.565 ± 0.058
0.377	0.289 ± 0.031
0.447	0.149 ± 0.017
0.517	0.069 ± 0.010
0.587	0.053 ± 0.008
0.658	0.029 ± 0.005
0.737	0.0078 ± 0.0014
0.833	0.0054 ± 0.0011
0.919	0.0013 ± 0.0004

5 Inclusive η production

In this section we present the results of η production by its reconstruction in the two photon decay mode. In order to suppress background photons dominantly due to π^0 decays, photon pairs in the range $70 \leqq m_{\gamma\gamma} \leqq 200$ MeV/c^2 were removed from the sample. The overall loss of η's due to removal of one or both of its decay photons in the above procedure is estimated to be about 8%.

The remaining photons with $E_\gamma \geqq 350$ MeV were then used for η reconstruction by calculating the invariant masses of all photon pairs. However, in order to further suppress uncorrelated photon combinations we demanded that:

1. The calculated energy asymmetry of each photon pair, A_η, defined as the difference of photon energies divided by their sum, should be less than 0.80,
2. Both photons of a pair must lie in the same hemisphere defined by a plane perpendicular to the sphericity axis of the event.

Due to the kinematics of the η decay the hemisphere cut affects only the very low energy photon pairs and becomes almost ineffective for $E_\eta \geqq 1.5$ GeV. The $\gamma\gamma$ mass spectrum of photons surviving these cuts is shown in Fig. 9a–c for three fractional energy bands x_η. Clear η signals are observed.

The η yield is extracted from the mass distributions by fitting a Gaussian plus a polynomial background in

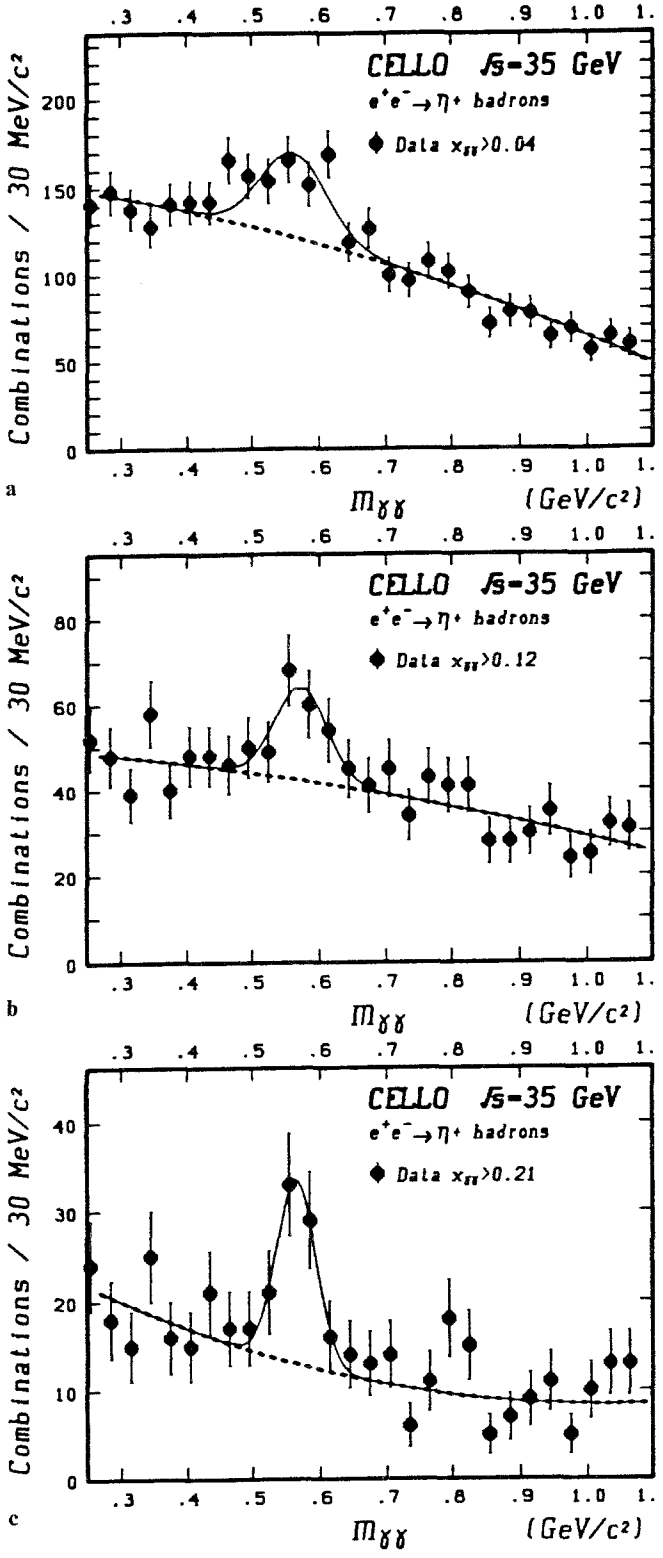

Fig. 9a–c. The invariant mass distribution of $\gamma\gamma$ combinations after π^0 removal for different energy ranges. The curves are the fit to signal and background

the interval $270 \leqq m_{\gamma\gamma} \leqq 900$ MeV/c^2. In the fit we left the width and the mean value as free parameters and obtained $\sigma_m = 30.1 \pm 6.5$ MeV/c^2, improving for higher η energies. The resultant mean of 558 ± 17 MeV/c^2 is very close to the true η mass 548 MeV/c^2. After background

Table 5. The scale invariant differential cross sections for inclusive η production in e^+e^- annihilation at $\sqrt{s}=35$ GeV. Errors are statistical only. See text for systematic errors

x_η	$\frac{s}{\beta}\frac{d\sigma}{dx_\eta}(\mu b \cdot \mathrm{GeV}^2)$
0.050	1.523 ± 0.285
0.105	1.011 ± 0.247
0.210	0.446 ± 0.216
0.375	0.143 ± 0.056
0.690	0.010 ± 0.003

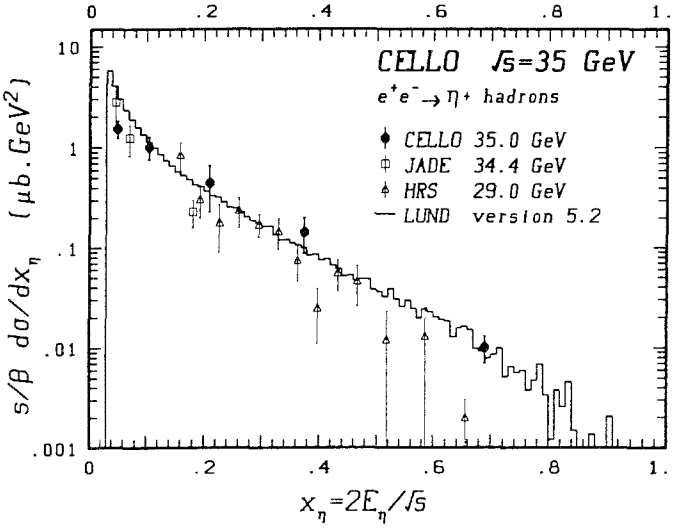

Fig. 10. The scale invariant differential cross section for η production

subtraction 272 ± 45 η's remain in the mass interval $450 \leqq m_{\gamma\gamma} \leqq 650$ MeV/c^2. For cross section calculations the fitting was done separately in 5 bins of x_η. The efficiency and radiative corrections were calculated in a similar way as described in the previous sections. In Table 5 and Fig. 10 we present the scale-invariant differential cross section for η production. The errors are statistical and include the uncertainities due to the fitting procedure. In addition to the systematic errors described in Sect. 3 we estimate an error of about 20% due to the applied cuts in the η reconstruction procedure, which is an average over the measured x range. The cross section is also compared with results from other experiments [6, 10]. There is reasonable agreement among different experiments concerning the yield as well as the slope of the spectra.

Using the CELLO measurements we determine the average η multiplicity per event to be $\langle N_\eta \rangle = 0.57 \pm 0.11 \pm 0.12$ in the range $x_\eta \geqq 0.04$ (i.e. corresponding to an energy cut of $E_\eta \geqq 700$ MeV). The prediction based on the LUND model in the same energy range yields $\langle N_\eta \rangle = 0.69$. Extrapolating our data to the kinematical limit we obtain $\langle N_\eta \rangle = 0.63 \pm 0.12 \pm 0.15$ to be compared to the value of $\langle N_\eta \rangle = 0.76$ predicted by the LUND model. The systematic error includes the uncertainty due to the Monte Carlo extrapolation to the full x range. There

is a reasonable agreement between the data and the LUND fragmentation model.

The measured multiplicity given above is also in good agreement with the JADE [6] at $\sqrt{s}=34.0$ GeV, the HRS [10] and MARK II [11] at $\sqrt{s}=29.0$ GeV, measurements of 0.64 ± 0.15, 0.58 ± 0.10 and 0.62 ± 0.17, respectively.

6 Conclusion

The inclusive production of γ, π^0 and η in electron-positron annihilation into hadronic final states has been investigated using the CELLO detector at PETRA at a center of mass energy of 35 GeV. The scale invariant differential cross sections are found to be in good agreement with our previous results and those of other experiments at similar energies. However, the π^0 momentum range presented here is considerably larger: The measurements of neutral pion cross sections were extended up to the kinematical limits using a method which efficiently identified and removed the single photon background. The average multiplicities of γ, π^0 and η are found to be $13.6\pm0.3\pm0.8$, $6.43\pm0.60\pm0.86$ and $0.63\pm0.12\pm0.15$, respectively. The neutral energy fraction in multihadronic events carried by photons is found to be 26.7%. We find the LUND fragmentation model in good agreement with our data.

Acknowledgements. We gratefully acknowledge the outstanding efforts of the PETRA machine group which made possible these measurements. We are indebted to the DESY computer centre for their excellent support during the experiment. We acknowledge the invaluable effort of the many engineers and technicians from the collaborating institutions in the construction and maintenance of the apparatus. The visiting groups wish to thank the DESY Directorate for the support and kind hospitality extended to them.

This work was partially supported by the Bundesministerium für Forschung und Technologie (Germany), the Commissariat à l'Energie Atomique and the Institut National de Physique Nucléaire et de Physique des Particules (France), the Science and Engineering Research Council (UK), and the Israeli Ministry of Science and Development.

References

1. CELLO Coll. H.J. Behrend et al.: Z. Phys. C – Particles and Fields 14 (1982) 189; CELLO Coll. H.J. Behrend et al.: Z. Phys. C – Particles and Fields 20 (1983) 207
2. CELLO Coll. H.J. Behrend et al.: Phys. Scr. 23 (1981) 610
3. B. Anderson et al.: Phys. Rep. 97 (1983) 33; Z. Phys. C – Particles and Fields 20 (1983) 317; T. Sjöstrand: Comp. Phys. Commun. 27 (1982) 243
4. EGS, R.L. Ford, W.R. Nelson: SLAC report 210 (1978)
5. HETC code, RISC Computer Code Collection, Oak Ridge National Laboratory, CCC-178
6. JADE Coll. W. Bartel et al.: Z. Phys. C – Particles and Fields 28 (1985) 343
7. CELLO Coll. H.J. Behrend et al.: Phys. Lett. 183B (1987) 400
8. CELLO Coll. H.J. Behrend et al.: Phys. Lett. 113B (1982) 427
9. TASSO Coll. M. Althoff et al.: Z. Phys. C – Particles and Fields 17 (1983) 5; TASSO Coll. W. Braunschweig et al.: Z. Phys. C – Particles and Fields 33 (1986) 13
10. HRS Coll. S. Abachi et al.: Phys. Lett. 205B (1988) 111
11. MARK II Coll. G. Wormser et al.: Phys. Rev. Lett. 61 (1988) 1057